

# Nano-hydroxyapatite preparation from biogenic raw materials

Research Article

Gréta Gergely<sup>1\*</sup>, Ferenc Wéber<sup>1</sup>, István Lukács<sup>1</sup>, Levente Illés<sup>1</sup>, Attila L. Tóth<sup>1</sup>, Zsolt E. Horváth<sup>2</sup>, Judit Mihály<sup>3</sup>, Csaba Balázs<sup>1</sup>

<sup>1</sup> Ceramics and Nanocomposites Department,  
Research Institute for Technical Physics and Materials Science,  
Hungarian Academy of Sciences, 1121 Budapest, Hungary

<sup>2</sup> Nanostructures Department,  
Research Institute for Technical Physics and Materials Science,  
Hungarian Academy of Sciences, 1121 Budapest, Hungary

<sup>3</sup> IR and Raman Spectroscopy Laboratory, Chemical Research Center,  
Hungarian Academy of Sciences, 1025 Budapest, Hungary

Received 26 August 2009; Accepted 10 November 2009

**Abstract:** Hydroxyapatite (HAp) was successfully produced from recycled eggshell, seashell and phosphoric acid. The phases obtained depended on the ratio of calcined eggshell/ seashell to phosphoric acid, the calcination temperature and the mechanochemical activation method (ball milling or attrition milling). The HAp structures were characterized by X-ray diffraction, scanning electron microscopy and infrared spectroscopy. Attrition milling was more effective than ball milling, yielding nanosize, homogenous and pure HAp.

**Keywords:** HAp • Raw material • Ball milling • Attrition • Characterization

© Versita Sp. z o.o.

## 1. Introduction

Hydroxyapatite,  $(\text{Ca}_{10}(\text{PO}_4)_6(\text{OH})_2)$  is chemically similar to the mineral component of bones and teeth [1-3]. HAp is among the few bioactive materials, meaning that it will support bone ingrowth and osseointegration when used in orthopaedic, dental and maxillofacial applications. Hydroxyapatite coatings are often applied to metallic implants, especially stainless steels and titanium alloys, to improve the surface properties. It may be employed in powders, porous blocks and hybrid composites to fill bone defects or voids when large sections of bone have had to be removed, or when bone augmentations are required (e.g. dental applications).

HAp can be produced from biogenic materials like coral [4], seashell, [5], eggshell [3,6,7], body fluids [8] and by some chemical synthetic methods. These are based on solid state reactions [9], chemical precipitation [10], hydrothermal reactions [11], sol-gel methods [12]

and mechanochemical methods [13,14] using different calcium and phosphorus-containing starting materials.

Hydroxyapatite nanopowders have been produced from eggshell and seashell-derived raw materials and phosphoric acid using a 1.67 Ca/P ratio [15]. The structures were characterized by X-ray diffraction (XRD) and scanning electron microscopy (SEM). The phases observed during the powder synthesis depended on the ratio of calcined eggshell/seashell to phosphoric acid, the calcination temperature, and the duration of the mechanochemical synthesis [7].

The present work aimed to synthesize HAp *via* mechanochemical activation with three objectives: (1) to form HAp from two different raw materials: eggshell and seashell; (2) to compare two mechanochemical activation process: ball milling and attrition milling; and (3) to study the phase stability and powder characteristics.

\* E-mail: gergelyg@mfa.kfki.hu

**Table 1.** Preparation parameters of hydroxyapatites.

Sample	Raw material	Milling		wt% shell : H <sub>3</sub> PO <sub>4</sub>	Milling time (h)	Sintering conditions	
		method	Rpm			Temperature (°C)	Holding time (h)
EA	eggshell	attrition milling	4000	50:50	5	-	-
EA_900				50:50	5	900	2
SA	seashell			50:50	5	-	-
SA_900				50:50	5	900	2
EB	eggshell	ball milling	350	50:50	10	-	-
EB_900				50:50	10	900	2
SB	seashell			50:50	10	-	-
SB_900				50:50	10	900	2

## 2. Experimental Procedure

Seashell and eggshell were collected and washed with detergent, then calcined in air at 900°C for 3 h. Every 10 minutes samples were removed for analysis. During the first 30 minutes most of the organic materials were burnt out, then the eggshell and seashell were converted to calcium oxide.

Calcined shells were crushed and milled in a ball mill or an attritor mill. The ball mill (Fritsch GmbH) was equipped with alumina balls and bowls, the attritor mill (Union Process) was fitted with zirconia tanks and zirconia balls (Ø2 mm). The crushed seashell or eggshell was reacted with phosphoric acid in an exothermic reaction. The mixtures were milled for 5 h at 4000 rpm (attritor milling) or for 10 h at 350 rpm (ball milling), to achieve homogenous mixtures and to prevent agglomeration. After milling, a small amount (approximately 0.5 g) of each type of HAp powder was sintered at 900°C for 2 h in air (Table 1). HAp powders usually degrade at high temperatures, the most common problem being CaO formation. The different types of shells and details of the milling procedure are presented in Table 1.

The powder phase composition was studied as a function of raw material and milling process by X-ray diffractometry (XRD - Bruker Advance 8D) and Fourier transform infrared spectroscopy (FTIR - Varian Scimitar FTIR spectrometer with broad band MCT detector). The morphologies of the calcined eggshell and seashell, of the synthesized powders, and of the heat treated powders were examined by scanning electron microscopy (SEM-LEO 1540 XB).

Elemental analysis was by energy dispersive X-ray spectroscopy (EDS-JEOL JSMIII 25) with a Bruker Si(Li) EDS detector and Quantax system. Collection times were typically 25-60 minutes (live time) using area scan mode on a single 1 mm<sup>2</sup> area. The data were converted to compositions using the Quantax no-standard P/B ZAF package.

## 3. Results and Discussion

The raw materials' morphologies after calcination are shown in Fig. 1. The eggshell structure (Fig. 1a) is more compacted than seashell; the average grain size is 2-3 µm. The seashell (Fig. 1b) possesses a more open structure containing 3-4 µm grains. Fig. 1c shows the XRD patterns of the raw materials. CaO (JCPDS-PDF 0371497) was observed in the calcined eggshell, CaO (JCPDS-PDF 0371497) and Ca(OH)<sub>2</sub> (JCPDS-PDF 0441481) in the calcined seashell.

The morphology of the powders made by attrition milling are shown in Fig. 2a - d while those produced by ball milling are shown in Figs. 2e - h. SEM micrographs show no significant difference between the eggshell (EA) and seashell (SA) morphologies (Figs. 2a, 2c). For both eggshell and seashell, attritor milling is more efficient in grain size reduction than ball milling. Thus, smaller particle size with homogeneous size distribution may be achieved with attritor milling. Grains in the SB and EB samples form micron size agglomerates (Figs. 2e, 2g).

After 900°C heat treatment, a 100 nm particle size is characteristic of both starting materials (Figs. 2b, 2d). Agglomerations can be found on Figs. 2f, 2h. Smooth surfaces are evolving after heat treatment at 900°C in both cases (EB\_900 and SB\_900).

Fig. 3 shows X-ray diffractograms of the powder samples. After intensive attrition milling EA and SA samples (Fig. 3a, 3b) contain hydroxyapatite (JCPDS-PDF 74-0565), calcite (CaCO<sub>3</sub>, JCPDS-PDF 05-0586), monetite (CaHPO<sub>4</sub>, JCPDS-PDF 071-1760) and phosphoric acid (H<sub>3</sub>PO<sub>3</sub>, JCPDS-PDF 072-0518). These four phases were observed in both eggshell (EA) and seashell (SA) samples. After heat treatment (900°C, 2h) the main phase was hydroxyapatite with some calcite and calcium oxide (CaO, JCPDS-PDF 037-1497) (EA\_900 and SA\_900).

Powders produced by ball milling (EB and SB) contained monetite, phosphoric acid, and portlandite

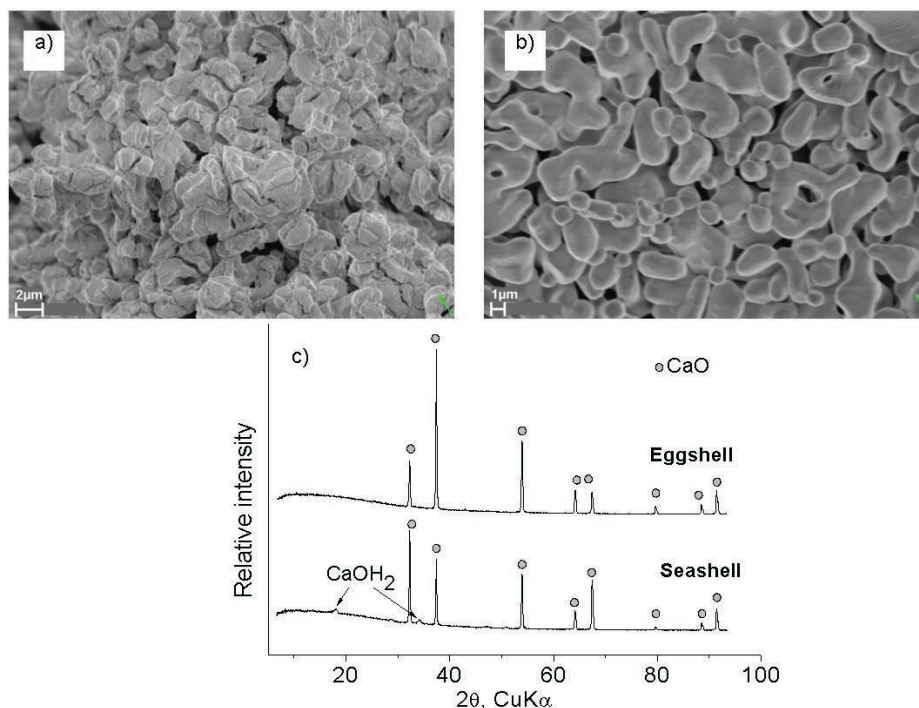


**Figure 1.** SEM images (a) eggshell and (b) seashell and XRD pattern of the calcinated material (c) eggshell and seashell.

**Table 2.** Elemental composition of hydroxyapatites.

Sample	O	Na	Mg	Si	wt%							Ca/P at.ratio
					P	S	Cl	Ca	Zn	Zr		
EA	42.05	0.08	0.45	0.06	16.01	0.1	0.03	41.01	0.06	0.16	1.98	
EA_900	31.76	0.05	0.47	0.1	18.34	0.1	0.01	48.98	0.06	0.14	2.06	
SA	41.83	0.1	0	0.16	15.72	0.06	0.03	41.93	0.04	0.11	2.06	
SA_900	27.89	0.11	0	0.15	18.95	0.03	0.01	52.52	0.05	0.29	2.14	
EB	49.67	0.01	0.4	0.03	14.81	0.09	0.01	34.87	0.06	0.05	1.82	
EB_900	41.25	0.06	0.47	0.07	16.85	0.08	0	40.99	0.04	0.17	1.88	
SB	37.63	0.2	0	0.09	17.08	0.02	0	44.77	0.07	0.16	2.03	
SB_900	35.73	0.28	0	0.13	17.63	0.03	0	46.16	0.04	0.01	2.02	

( $\text{Ca}(\text{OH})_2$ , JCPDS-PDF 044-1481) (Figs. 3c, 3d). In contrast to attrition milled samples the HAp phase was not detected before heat treatment.

After heating at 900°C for 2 h hydroxyapatite, CaO, and calcite appeared in both EB\_900 and SB\_900 samples, independent of the raw material. In the EB\_900 sample, calcium phosphate ( $\beta\text{-Ca}_3(\text{PO}_4)_2$ , JCPDS-PDF 70-2065) and whitlockite ( $\text{Ca}_3(\text{PO}_4)_2$ , JCPDS-PDF 002-0786) were observed. Calcium phosphate ( $\beta\text{-Ca}_3(\text{PO}_4)_2$ , JCPDS-PDF 005-0586) was found in the SB\_900 powder.

In order to check the presence of elements in addition to the diffractograms energy dispersive X-ray microanalysis (EDS) measurements were performed on the milled powder samples. As the hydrogen content can not be analyzed by X-ray methods, furthermore

the irregular and porous samples do not allow rigorous correction of the EDS spectra, the results can be considered as semiquantitative ones. The spectra were collected in a JSM-25 S-III SEM using Bruker Si(Li) EDS detector and Quantax system using area scan mode for averaging. The collection times were typically 25-60 minutes (live time) on a single 1 mm<sup>2</sup> area of each sample, then the data were turned into numerical composition values using the no-standard P/B ZAF package of the Quantax system. The normalized mass percent output values of the P/B ZAF program are summarized in Table 2. Zirconia may be found in the samples prepared by attrition milling only, because of wearing of zirconia milling parts (balls, tanks). Other elements found by EDS are sodium and silicon (as shown in Table 2). These elements are characteristic

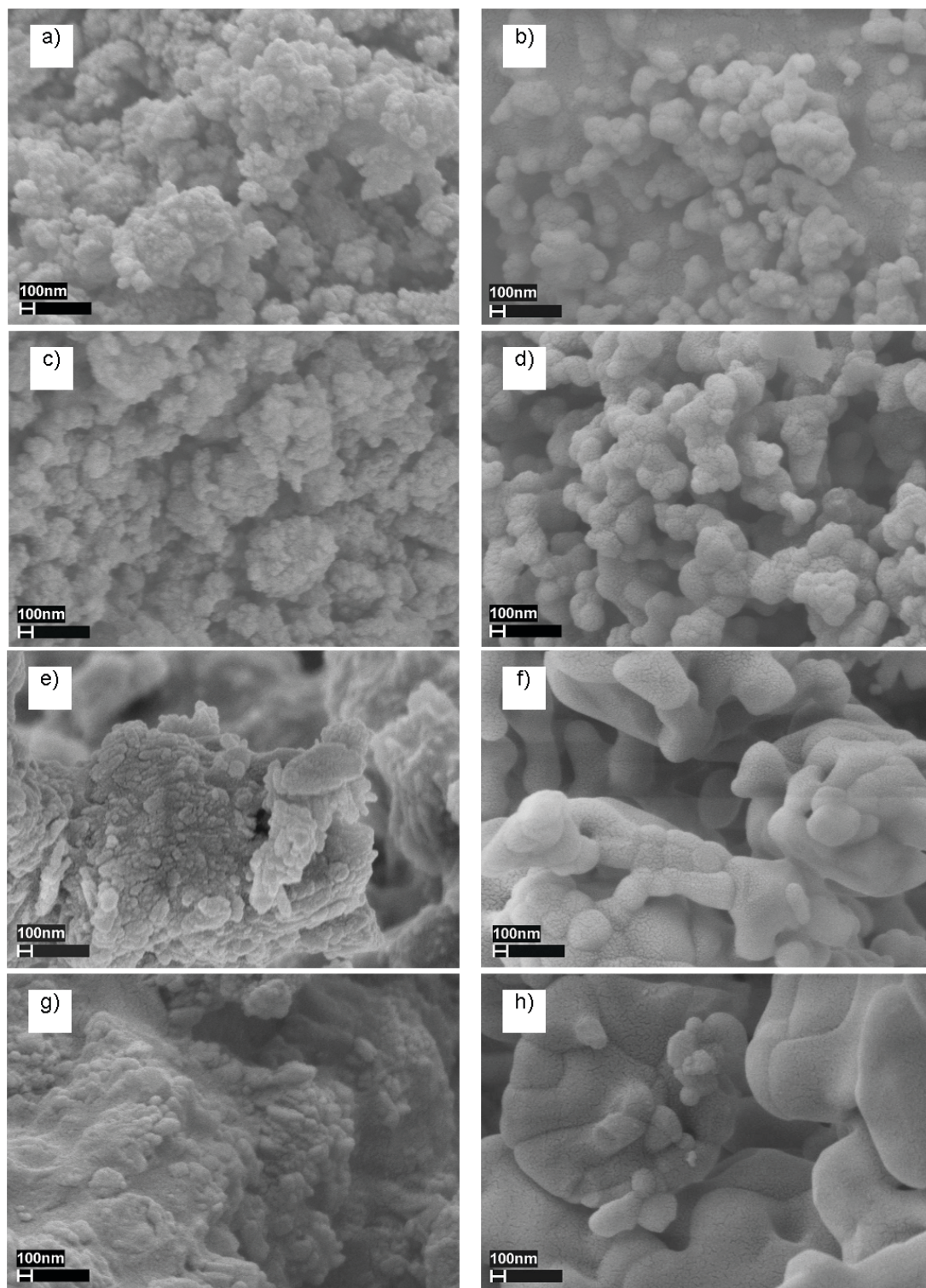


**Figure 2.** SEM micrographs of attrition ((a) EA,(b) EA\_900,(c) SA,(d) SA\_900) and ball ((e) EB ,(f) EB\_900,(g) SB,(h) SB\_900) milled samples.

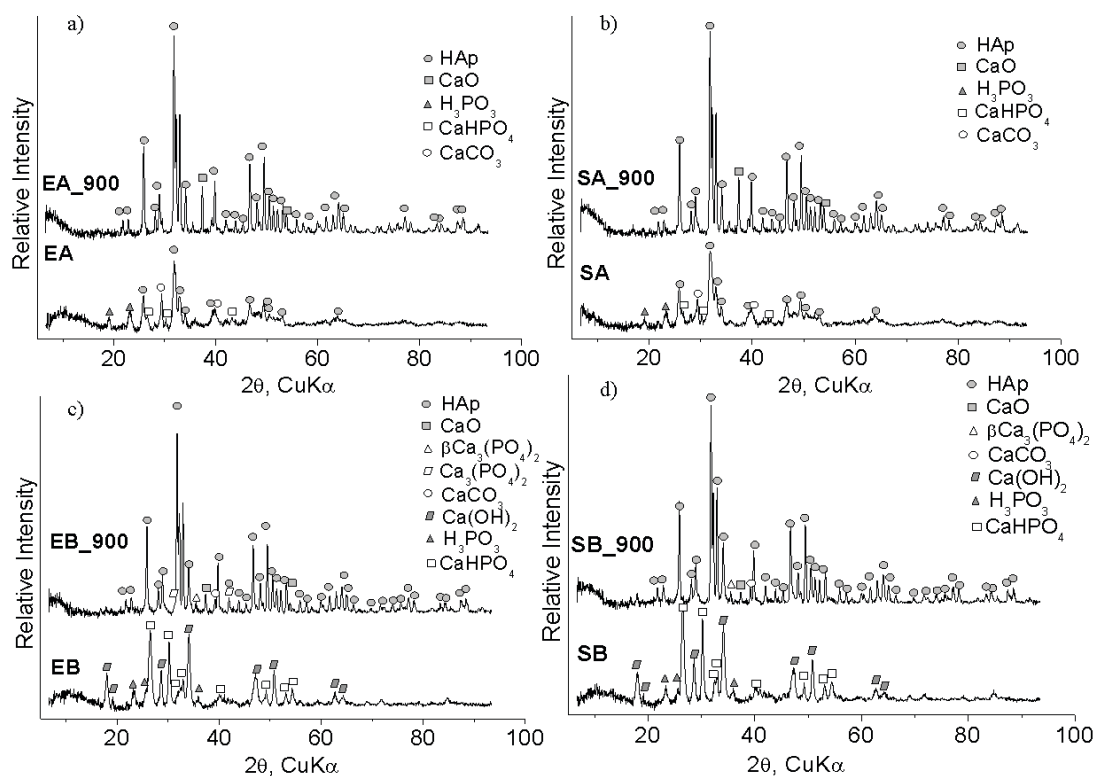


**Figure 3.** X-ray diffractograms of the samples: (a) EA and EA\_900, (b) SA and SA\_900, (c) EB and EB\_900, (d) SB and SB\_900.

trace elements of eggshell and seashell. Sulphur and chlorine are other contaminants. As observed by EDS the chlorine can be found only in attrition milled samples. Although the EDS results are semiquantitative ones, it is interesting to see that magnesium is found in the eggshell samples only, whereas the sodium is more characteristic for seashell samples.

The FTIR spectrum of the EB sample after ball milling (Fig. 4b) shows a complex mixture of calcium phosphate phases:  $\text{CaHPO}_4$ ,  $\text{Ca}_3(\text{PO}_4)_2$  and  $\text{Ca}_{10}(\text{PO}_4)_6(\text{OH})_2$ . Fig. 4a shows the FTIR spectrum of seashell (SB) after ball milling. Beside organic residues, the spectrum is dominated by  $\nu\text{OH}$  at  $3640\text{ cm}^{-1}$ , assigned to surface hydroxyl groups and to  $\text{CaHPO}_4$ .

After heating at  $900^\circ\text{C}$  (SB\_900) well-crystallised hydroxyapatite with some carbonate substitution can be observed ( $\nu_3\text{PO}_4$  at  $1087$  and  $1016\text{ cm}^{-1}$ ,  $\nu_1\text{PO}_4$  at  $962\text{ cm}^{-1}$  and the triplet of  $\nu_4\text{PO}_4$  at  $631$ ,  $598$  and  $565\text{ cm}^{-1}$ ). The band at  $539\text{ cm}^{-1}$  can be assigned to acid phosphate ( $\text{HPO}_4^{2-}$ ) in the mineral phase. This band decreases in matured bone apatite and in highly crystalline hydroxyapatite [13,14]. The pure hydroxyapatite phase with some carbonate substitution is formed only after  $900^\circ\text{C}$ . However, surface OH bands are also present in the spectrum.

After heat treatment (EB\_900), apatite spectral features become dominant - above  $800\text{-}900^\circ\text{C}$  typical

bands of well-crystallised hydroxyapatite appear ( $\nu_3\text{PO}_4$  at  $1086$  and  $1018\text{ cm}^{-1}$ ,  $\nu_1\text{PO}_4$  at  $961\text{ cm}^{-1}$  and the  $\nu_4\text{PO}_4$  triplet at  $626$ ,  $599$  and  $561\text{ cm}^{-1}$ ) as well as carbonate ( $\nu_3$  at  $1466$  and  $1409\text{ cm}^{-1}$ ,  $\nu_2$  at  $874\text{ cm}^{-1}$ ,  $\nu_4$  at  $713\text{ cm}^{-1}$ ) and surface OH ( $3640\text{ cm}^{-1}$ ) peaks [15,16]. No traces of  $\text{HPO}_4^{2-}$  ( $540\text{-}530\text{ cm}^{-1}$ ), characteristic of immature bone mineral or incomplete apatite formation can be observed [15].

The spectrum after attrition milling (EA) (Fig. 4c) resembles that of bone mineral. It is dominated by typical  $\text{PO}_4$  bands of poorly crystalline apatite (triply degenerate  $\nu_3\text{PO}_4$  asymmetric stretch at  $1021$  and  $1087\text{ cm}^{-1}$  (shoulder), non-degenerate symmetric stretch of  $\nu_1\text{PO}_4$  at  $962\text{ cm}^{-1}$ , and components of the  $\nu_4\text{PO}_4$  bending triplet at  $599$  and  $562\text{ cm}^{-1}$  [13,16]. Carbonate bands are also observed at  $1550\text{-}1350\text{ cm}^{-1}$  ( $\nu_3$ ),  $873\text{ cm}^{-1}$  ( $\nu_2$ ) and  $712\text{ cm}^{-1}$  ( $\nu_4$ ). By analogy with bone mineral, the position of carbonate bands ( $1456$ ,  $1415$  and  $872\text{ cm}^{-1}$ ) indicates the formation of a carbonated apatite with B-type substitution (in tetrahedral positions) [17]. The broad, weak  $3000\text{-}3400\text{ cm}^{-1}$  band can be attributed to traces of water, confirmed by the very weak, broad H-O-H bend around  $1640\text{ cm}^{-1}$ . In the OH stretching vibration region appear both hydroxyapatite  $\nu\text{OH}$  and surface OH at  $3644\text{ cm}^{-1}$ , probably connected to surface CaO. The surface OH band also increases with increasing temperature (EA\_900).

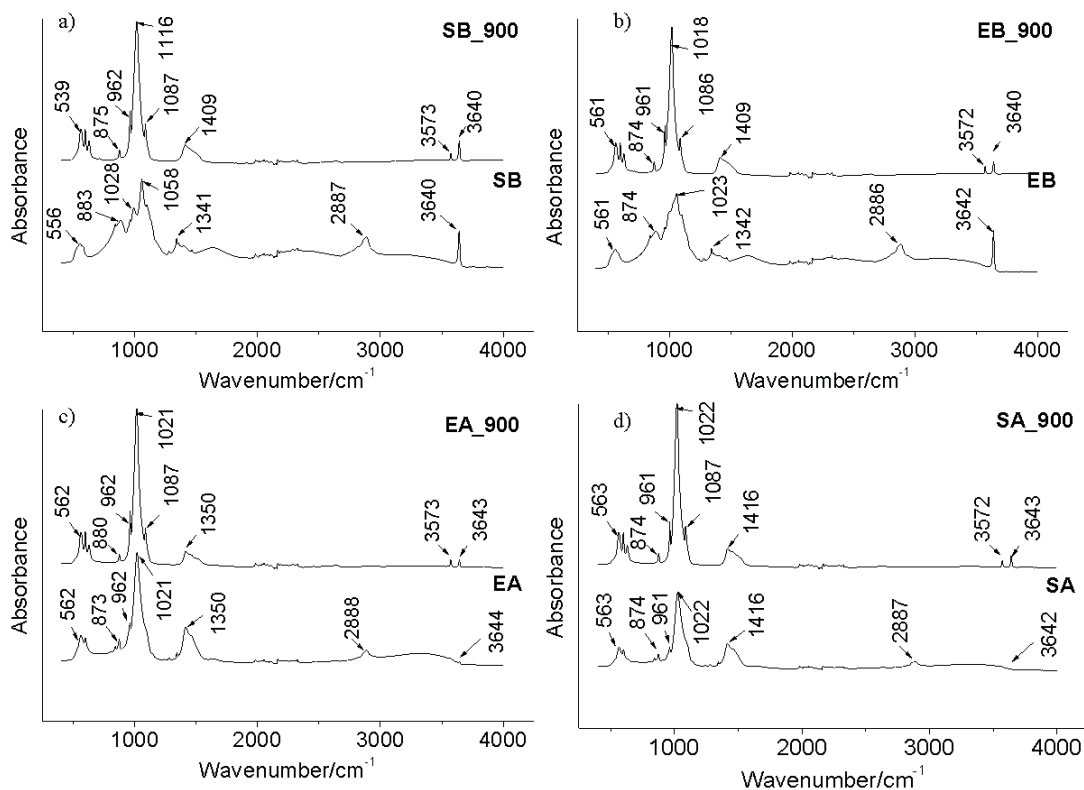


**Figure 4.** FTIR spectra of the samples: a) SB and SB<sub>900</sub>, b) EB and EB<sub>900</sub>, c) EA and EA<sub>900</sub>, d) SA and SA<sub>900</sub>.

The SA spectrum (Fig. 4d) also resembles that of bone mineral, dominated by poorly crystalline apatite. Similar to EA, the carbonate bands indicate the formation of a B-type substituted carbonated apatite. The peaks marked with an asterisk belong to organic residues (ethanol was used during milling). As for sample EA, hydroxyapatite  $\nu$  OH and surface OH, probably connected to CaO, are present. With increasing temperature (SA<sub>900</sub>) carbonate decreases and the spectral features of well-crystallised hydroxyapatite dominate, with splitting of  $\nu_3$  and  $\nu_4$  PO<sub>4</sub>.

## 4. Conclusions

For both eggshell and seashell samples ball milling resulted in micrometer sized aggregated coarse grains with smooth surfaces, while attrition milled samples

are characterized by nanometer size grains. The characteristic morphology is preserved even after firing at high temperature (900°C). Samples after ball milling include little or no Hap, but attrition milling yielded mainly Hap. After heat treatment HAP, calcium oxide and calcium phosphate phases appeared in both cases.

Attrition milling was much more effective than ball milling. Nanosized, homogeneous HAP resulted before heat treatment.

## Acknowledgement

Thanks to OTKA grant 76181 and Hungarian – South –Korea bilateral TÉT project.

## References

- [1] E. Saiz et al., *Mat. Sci. and Eng. C* 27, 546 (2007)
- [2] K. de Groot, *Biomaterials* 1, 47 (1980)
- [3] E.M. Rivera et al., *Mat. Lett.* 41, 128 (1999)
- [4] U. Ripamonti, J. Crooks, L. Khoali, L. Roden, *Biomaterials* 30, 1428 (2009)
- [5] S.Kenneth et al., *Acta Biomater.* 3, 910 (2007)
- [6] S.J. Leea, S.H. Oh., *Mat. Lett.* 57, 4570 (2003)
- [7] Cs. Balázsai et al., *J. Eur. Cer. Soc.* 27, 1601 (2007)
- [8] A. CuK neyt Tas, *Biomaterials* 21, 1429 (2000)
- [9] X. Yang, Z. Wang, *J. Mater. Chem.* 8, 2233 (1998)
- [10] D. Tadic, F. Peters, M. Epple, *Biomaterials* 23, 2555 (2002)

- [11] S. Jinawath, D. Polchai, M. Yoshimura, *Mater. Sci. and Eng. C* 22, 35 (2002)
- [12] C.S. Chai, K.A. Gross, B.B. Nissan, *Biomaterials* 19, 2291 (1998)
- [13] B. Nasari-Tabrizi *et al.*, *Mat. Lett.* 63, 543 (2009)
- [14] K.C.B. Yeong, J. Wang, S.C. Ng, *Biomaterials* 22, 2705 (2001)
- [15] Cs. Balázsi *et al.*, *Mat. Sci. For.* 537-538, 105 (2007)
- [16] K.C.B. Yeong, J. Wang, S.C. Ng, *Biomaterials* 22, 271 (2001)
- [17] A. Slosarczyk, E. Stobicrska, Z. Paszkiewicz, M. Gawlicki, *J. Am. Ceram. Soc.* 79, 2539 (1996)
- [18] N.O. Engin, A.C. Tas, *J. Am. Ceram. Soc.* 83, 1581-1584 (2000)
- [19] L. M. Miller *et al.*, *Biochim. et Biophys. Acta* 1527, 11 (2001)
- [20] F.Z. Zakaria *et al.*, *J. Raman Spectrosc.* 39, 1204 (2008)
- [21] V.C. Farmer, *The Infrared Spectra of Minerals* (Bartholomew Press, Dorking, Surrey, 1974) 390
- [22] A. Slosarczyk *et al.*, *Cer. Inter.* 23, 297 (1997)
- [23] C. Rey, V. Renugopalakrishnan, B. Collins, M.J. Glimcher, *Calcif. Tissue Int.* 49, 251 (1991)